

Investigation of Umbral Dots with the New Vacuum Solar Telescope

Kaifan Ji¹ · Xia Jiang^{1,2} · Song Feng^{1,2} ·
Yunfei Yang^{1,2} · Hui Deng¹ · Feng Wang¹ ·

© Springer ●●●

Abstract

Umbral dots (UDs) are small isolated brightenings observed in sunspot umbrae. They are convective phenomena existing inside umbrae. UD are usually divided into central UD (CUDs) and peripheral UD (PUDs) according to their positions inside an umbra. Our purpose is to investigate UD properties and analyze their relationships, and further to find whether or not the properties depend on the umbral magnetic field variation. For this purpose, we selected the high-resolution TiO images of four active regions (ARs) obtained under the best seeing conditions with the *New Vacuum Solar Telescope* in the Fuxian Solar Observatory of the Yunnan Astronomical Observatory, China. The four ARs (NOAA 11598, 11801, 12158, and 12178) include six sunspots. A total of 1220 CUDs were identified in six sunspots, and 603 PUDs in three sunspots. Meanwhile, the radial component of the magnetic field of the sunspots obtained with the *Helioseismic and Magnetic Imager* onboard the *Solar Dynamics Observatory* was used to analyze the relationship between UD properties and the magnetic field. The diameters and lifetimes of CUDs exhibit an increasing trend with brightness, whereas their horizontal velocities exhibit an inverse trend. Moreover, the diameter, intensity and velocity depend on the magnetic field variation. The diameter of a CUD becomes larger and brighter, and its motion slower in a weak magnetic field than in a strong field. Similar trends are also found for PUDs. Moreover, we also find that the lifetimes of UD located in different sunspots are not obviously different, implying that they are unrelated to the magnetic flux density in which they live.

Keywords: Sunspots, Umbra; Sunspots, Magnetic Fields

¹ Faculty of Information Engineering and Automation /
Yunnan Key Laboratory of Computer Technology
Application, Kunming University of Science and Technology,
Kunming 650500, China email: ynkmsf@escience.cn
² Key Laboratory of Solar Activity, National Astronomical
Observatories, Chinese Academy of Sciences, Beijing
100012, China

1. Introduction

There are some small bright features called umbral dots (UDs) in a dark umbra, and the features can be found almost all over umbrae and pores. UD only cover 3–10 % of the umbral area, but contribute 10–20 % of the brightness (Sobotka, Bonet, and Vazquez, 1993). This implies that convective motions must exist within umbrae because radiation cannot explain the phenomena. Therefore, UD play a vital role in the energy balance of sunspots. The study of UD is crucial to understand the convective motions and the interactions of the plasma with strong magnetic fields, and analyze the formation mechanism of sunspots. Usually, UD are generally divided into two classes according to their origin (Grossmann-Doerth, Schmidt, and Schroeter, 1986). UD are called peripheral UD (PUDs) near the penumbra-umbra boundary and central UD (CUDs) in the umbral center. PUDs are generally brighter than CUDs, and move quickly toward the center of the umbra, however, CUDs are relatively static. Two different models have been proposed to explain the formation mechanism of UD: the clustered magnetic flux tube and the monolithic flux tube model. The former considers that UD are a hot field-free gas intruded into a cluster of magnetic flux tubes (Parker, 1979). The latter suggests that the energy transport in an umbra is dominated by non-stationary narrow rising plumes of hot plasma with adjacent downflows. The UD are formed by the narrow upflow plumes that become almost field-free near the surface layer (Schüssler and Vögler, 2006). The essential difference between the two models is that the boundary of UD exists the local downflows in the monolithic flux tube model. Detail studies of the physical properties of UD, such as morphology, velocity, lifetime, and intensity, and the relationships between different properties are crucial to understanding the nature of the local convective motions (Sobotka, Brandt, and Simon, 1997a,b; Bharti, Joshi, and Jaaffrey, 2007; Riethmüller *et al.*, 2008; Watanabe *et al.*, 2012).

Our aim is to analyze the properties of UD, and the relationships between different properties, and further to find whether or not the properties depend on the umbral magnetic field variation. So we selected the high-resolution observations of four active regions (ARs) obtained under the best seeing conditions with the New Vacuum Solar Telescope (NVST) in the Fuxian Solar Observatory of the Yunnan Astronomical Observatory, China. The four ARs include six sunspots.

The layout of the paper is as follows. The observations and data reduction are described in Section 2. Section 3 briefly describes the identification procedure of CUDs and PUDs. Section 4 illustrates the physical properties of CUDs and PUDs, and their relationships. Moreover, the relationship between UD properties, and the relationship between the properties and the magnetic field are discussed. Finally, we give our conclusions in Section 5.

2. Observations and Data Reductions

The NVST is a vacuum solar telescope with a 985 mm clear aperture whose aims are to obtain high-resolution imaging and spectral observations, including

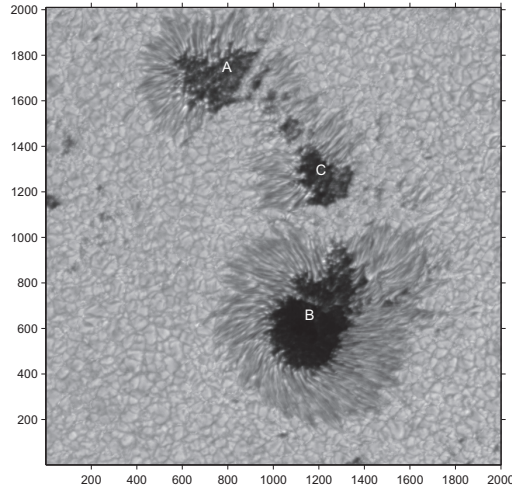


Figure 1. A corrected image of NOAA 12158, whose original image was recorded on 13 September 2014 at 03:00:00 UT with the NVST. The active region included three sunspots marked as A, B and C.

measurements of the solar magnetic field. The telescope consists of one channel for the chromosphere and two channels for the photosphere. The band used for observing the chromosphere is $H\alpha$ (656.3 ± 0.025 nm). The bands for observing the photosphere are the TiO (705.8 ± 1 nm) and the G-band (430.0 ± 0.8 nm). The high-resolution data of the NVST are classified into two levels. The level 1 data are processed by frame selection (lucky imaging) (Tubbs, 2004). The level 1+ data are reconstructed by speckle masking (Lohmann, Weigelt, and Wirtz, 1983) or iterative shift and add (Zhou and Li, 1998). Technical details of the NVST were described by Liu *et al.* (2014) and Xu *et al.* (2014).

Because the TiO line is highly sensitive to umbral temperature variations (Berdyugina, Solanki, and Frutiger, 2003), the observations of the band are more appropriate to investigating UDs. Therefore, we used the level 1+ TiO observations, rather than the $H\alpha$ and G-band ones. We selected the high-resolution images of six sunspots based on the best seeing conditions since October 2012. They were obtained from four active regions: NOAA 11598, 11801, 12158, and 12178. The observation parameters are listed in Table 1. The high-resolution data were obtained without adaptive optics. In good seeing conditions, without adaptive optics, the resolution of the reconstructed images can almost reach high-angular resolution near the diffraction limit of the NVST (Liu *et al.*, 2014).

The images in each sequence were coaligned by a subpixel registration algorithm (Feng *et al.*, 2012; Yang *et al.*, 2015). From Table 1 we can see that the sunspots of NOAA 11598, 11801, 12158 were away from the solar disk center, especially the sunspot located in NOAA 11801. Its heliocentric angle, θ , was close to 39° (*i.e.*, $\cos(\theta)=0.78$). So we used the SolarSoft routine `wcs_convert_from_coord` to transform the images of NOAA 11598, 11801, 12158 to heliographic coordinate for correcting the projection effects (Sun, 2013). Figure 1 shows a corrected

Table 1. Parameter of the observed sunspots

AR NOAA	Date	Time interval (UT)	Location	Pixel size (")	Cadence(s)
11598	29-10-2012	05:50:13–07:44:36	S11W27	0.041	37
11801	01-08-2013	03:38:35–04:34:55	W31N24	0.041	20
12158	13-09-2014	02:57:30–03:47:14	N20W27	0.052	30
12178	03-10-2014	04:35:00–05:33:03	S01E05	0.052	40

sample of NOAA 12158 obtained at 03:00:00 UT on 13 September 2014, where three sunspots (A, B and C) are presented.

3. Identification and Tracking of UD

We followed the method discussed in Feng *et al.* (2015) to identify and track CUDs and PUDs. The method mainly consists of three steps: firstly, the periphery and center boundary inside the umbra are detected based on the morphological reconstruction technique; secondly, the UD are identified based on the phase congruency technique; finally, the identified UD are tracked based on a 26-connected neighborhood technique. The phase congruency technique has been used to extract those low-contrast solar features, like coronal loops and umbral flashes (Feng *et al.*, 2014a,b).

Usually, empirical distance thresholds have been used to divided UD into CUDs and PUDs (Riethmüller *et al.*, 2008; Watanabe, Kitai, and Ichimoto, 2009; Hamedivafa, 2011; Louis *et al.*, 2012). Riethmüller *et al.* (2008) considered an UD as a PUD if the UD’s birth position is closer than 400 km from a defined umbra boundary, otherwise it is defined as a CUD. Hamedivafa (2011) defined a narrow width near the umbral boundary using an empirical threshold within which the UD are considered as PUDs. Louis *et al.* (2012) considered UD with a threshold 0.8" inward from an assigned umbra boundary as PUDs, and those located outward as CUDs.

Because the definition of the periphery and center boundary is crucial to investigating UD, we briefly introduce the definition and the identification procedure proposed by Feng *et al.* (2015). They defined the periphery and center boundary according to the umbral profile. We drew a three-dimension surface of a corrected image obtained from NOAA 11801 and show it in Figure 2. As illustrated with a red dash-line, the profile of the umbra can be approximated by a trapezoid whose two sides appear skew, and the base is relatively flat. Thus, the base of the trapezoid is defined as the center of the umbra, in which the UD are considered as CUDs. The two skew sides of the trapezoid are defined as the region of PUDs, *i.e.*, both sides. For obtaining the periphery and center boundary of each image, the image is first reconstructed by the morphological reconstruction technique, and then two thresholds are used to extract the periphery and center. In this

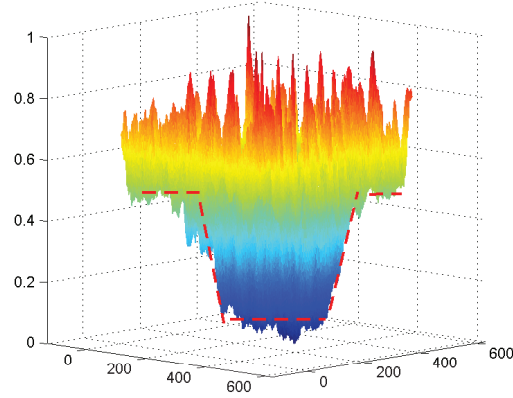


Figure 2. The surface of a corrected example whose original image was obtained at 03:48:04 UT on 1 August 2013. The red dash-line illustrates the umbral profile that can be approximated by a trapezoid.

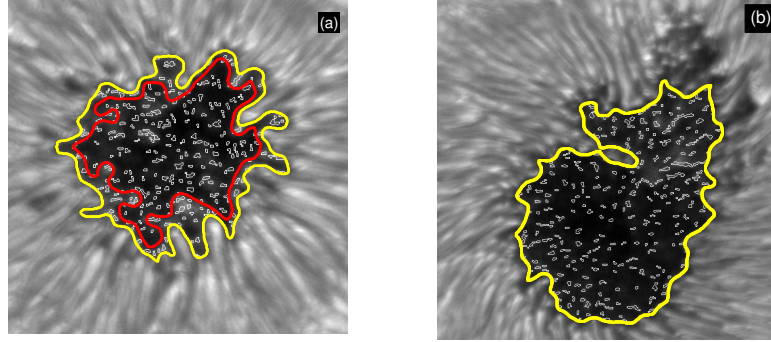


Figure 3. The identified UD using the method proposed by Feng *et al.* (2015). (a) The identified UD in a corrected sample image from NOAA 11801 whose original image was obtained at 03:48:04 UT on 1 August 2013. (b) The identified UD from the sunspot marked as B in Figure 1. The umbra-penumbra and periphery-center boundaries are indicated with red and yellow curves, respectively, and the identified UD are marked with white closed curves.

example, the thresholds, 0.3 and 0.6 R_{max} , were used to identify the regions. R_{max} denotes the maximum intensity of the reconstructed image.

Two examples including the identified UD, and the periphery and center boundaries are shown in Figure 3. The periphery and center boundaries are marked with yellow and red curves, respectively, and the positions of the identified UD are marked with white closed curves. We only extracted CUDs, without PUDs, from the three sunspots of NOAA 12158. Therefore, we extracted CUDs from six sunspots and PUDs from three sunspots.

Table 2. The number of the identified UD of each sunspot

AR NOAA	11598	11801	12158			12178
Spot			A	B	C	
CUD	313	201	90	279	75	262
PUD	219	162	0	0	0	222

4. Results and Discussion

Firstly, the statistical properties of UDs such as equivalent diameter, ratio of the maximum intensity to the mean intensity of the corresponding adjacent umbral background, horizontal velocity, and lifetime are obtained. Secondly, the intensity-diameter, lifetime-diameter, lifetime-intensity, and velocity-intensity relationships are analyzed. Finally, the relationships between UD properties, and the relationship between UD properties and the magnetic field intensity are discussed.

4.1. Property Definition and Feature Extraction

For each UD, its equivalent diameter (D_{eq}) is calculated as $\sqrt{4A/\pi}$, where A denotes the total number of pixels of an UD. The coordinate (x_c, y_c) of the centroid and the ratio of the maximum intensity (I_{ud}) to the mean intensity of the adjacent umbral background (I_{bg}) are determined from the identified areas. Some UD properties are defined using the tracking procedure; these are: the tracking procedure: lifetime (T_{ud}), birth-death distance (L_{bd}), and horizontal velocity (V_{ud}). T_{ud} is the sum of the cadence of all frames. L_{bd} is the centroid distance in its birth frame to its death frame. The horizontal velocity, V_{ud} , is the ratio of L_{bd} to T_{ud} .

We rejected the UDs whose diameter is lower than 130 km (0.18") and lifetime less than two minutes for accurate statistical results. In the tracking procedure, if splitting or merging occurred, the UD was discarded. Finally, a total of 1220 CUDs and 603 PUDs were obtained. Table 2 lists the number of CUDs and PUDs of each sunspot. In the following we utilize the UDs to analyze their physical properties and the relationships among the different properties and the magnetic field.

4.2. Statistical Properties of UDs

Figure 4 shows the statistical properties and corresponding fitted curves of the CUDs and the PUDs located in AR NOAA 12178; other ARs are not shown due to the similar distributions and fit curves. However, all the statistical results are listed in Table 3. Red color indicates the CUDs statistics and blue color indicates those of PUDs in Figure 4. Their corresponding fit functions are indicated with

Table 3. The statistical values of the CUD and PUD properties

CUDs					
NOAA	Spot	Diameter(km)	I_{ud}/I_{bg}	Lifetime(min)	Velocity(km s ⁻¹)
11598		178±40	1.05±0.02	5.35	0.37±0.19
11801		216±38	1.07±0.03	4.48	0.30±0.16
12158	A	235±41	1.10±0.05	5.67	0.27±0.14
12158	B	225±40	1.08±0.04	5.66	0.38±0.20
12158	C	234±45	1.09±0.04	7.26	0.19±0.10
12178		210±38	1.07±0.03	4.59	0.37±0.19
PUDs					
11598		195±41	1.08±0.06	6.25	0.47±0.24
11801		226±46	1.15±0.09	7.95	0.45±0.24
12178		226±41	1.12±8.12	4.59	0.51±0.27

the corresponding color curves. In this Figure, the unit of the Y axis is the corresponding probability density function (PDF) of each property.

Figure 4a shows the histograms of the equivalent diameters, and their distribution functions. The histograms are fitted using Gaussian functions. The diameter of CUDs ranges from 179 to 235 km, and that of PUDs from 195 to 226 km. The results are in a good agreement with those of previous works (Hamedivafa, 2008; Riethmüller *et al.*, 2008; Bharti, Beeck, and Schüssler, 2010; Kilcik *et al.*, 2012). These authors found that the UD diameters range between 150 and 350 km.

Figures 4b shows the histogram of the ratio (I_{ud}/I_{bg}), and its fitted distribution. Gaussian functions are used to fit the distributions. From Table 3, we see that the intensity ratio of CUDs ranges from 1.05 to 1.10 and that of PUDs from 1.08 to 1.15. This implies that the brightness of CUDs is 5–10 % higher than that of their adjacent background, and 8–15 % for PUDs.

As shown in Figure 4c, the histograms of the CUDs and PUDs lifetimes appear to follow an exponential distribution, so we used exponential functions to fit them. The variation range of the UD lifetimes is between four and seven minutes. The exponential distribution is in qualitative agreement with other works in the literature (Sobotka *et al.*, 1999; Riethmüller *et al.*, 2008; Hamedivafa, 2011; Feng *et al.*, 2015).

Because the horizontal velocities of the UDs, regardless of CUDs and PUDs, in the East–West and North–South directions on the Sun exhibit Gaussian distributions, we used Rayleigh functions to fit them. The velocity range of CUDs is between 0.19 and 0.38 km s⁻¹ and that of PUDs between 0.47 and 0.51 km s⁻¹

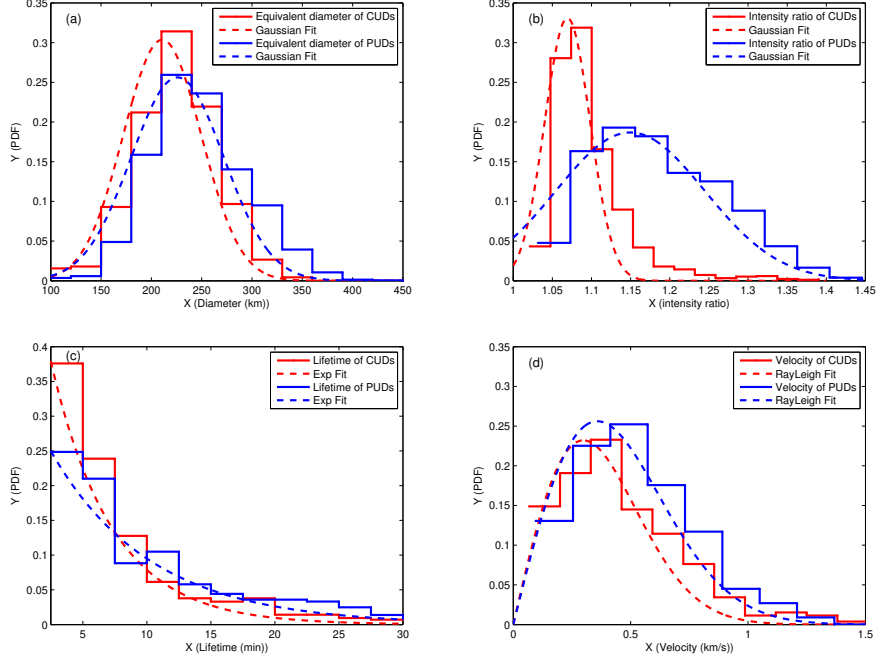


Figure 4. The histograms and the distribution curves of the CUDs and PUDs located in the sunspot of NOAA 12178. (a) Equivalent diameter, (b) intensity ratio, (c) lifetime, and (d) horizontal velocity. The red color indicates the statistics of CUDs, and the blue color those of PUDs. The Y axis indicates the corresponding probability density function (PDF) of each property.

(see Table 3). The velocities of CUDs and PUDs are also remarkably different; the horizontal velocity of CUDs is slower than that of PUDs. Our findings are in agreement with the articles by Watanabe, Kitai, and Ichimoto (2009) and Kilcik *et al.* (2012). These authors concluded that PUDs have a relatively fast horizontal velocity because they are located in regions with a strong horizontal component of the magnetic field and/or strongly inclined fields.

4.3. Correlation Analysis of UD Properties

The relationships, such as intensity-diameter, lifetime-diameter, lifetime-intensity, and velocity-intensity, for all CUDs (1220, obtained from six sunspots) and all PUDs (603, from three sunspots) are presented in the form of scatter plots in Figure 5. In the panels of this figure, the green lines are the standard errors of each bin, and the solid red lines are the fitted lines based on the bins. In this figure, the data were divided into 15 groups according to the minimum and maximum values along the X axis, and each group is a bin. Note that this division can result in very little or no data in a bin. As shown in Figure 5d, only five bins are shown although originally we considered 15 groups. The corresponding correlation coefficients are listed in Table 4. In the panels in the left column of Figure 5, we see that the relationships intensity-diameter (Figure

Table 4. The correlation coefficients of CUDs and PUDs

	Intensity-Diameter	Lifetime-Diameter	Lifetime-Intensity	Velocity-Intensity
CUD	0.62	0.38	0.33	-0.19
PUD	0.55	0.47	0.48	-0.19

5a), lifetime-diameter (Figure 5c), and lifetime-intensity (Figure 5e) exhibit an increasing trend; however, the relationship velocity-intensity (Figure 5g) shows a decreasing trend. The results indicate that larger CUDs tend to be brighter, live longer and move slower. Although the trend can be found for PUDs (see the panels in the right column of Figure 5), we are not sure about it, because only three spots were included in the sample.

Bharti, Beeck, and Schüssler (2010) concluded from realistic radiative MHD simulations that the relationships area-lifetime and brightness-lifetime are positively correlated. They stated that the correlations exist due to the fact that stronger and more extended convective upflows are maintained longer and create larger and brighter UD. Similar trends were found by the authors (Tritschler and Schmidt, 2002; Sobotka and Puschmann, 2009; Kilcik *et al.*, 2012). Kilcik *et al.* (2012) studied the statistical properties of UDs using high-resolution observations recorded by the *New Solar Telescope* at the Big Bear Solar Observatory and three-dimensional MHD simulations of sunspots. They concluded that the UD velocities are inversely related to their lifetimes. Our finding about the CUD trends also supports the results.

4.4. Relationship Between UD Properties and the Umbral Magnetic Field

In order to analyze the relationship between UDs properties and umbral magnetic field, we obtained the radial component of the magnetic field, B_r for the six sunspots observed with the *Helioseismic and Magnetic Imager* onboard the *Solar Dynamics Observatory* (SDO/HMI, Schou *et al.*, 2012). Because the HMI image pixel-scale is 0.5" and UD diameters approximate 0.3" (Schüssler and Vögler, 2006; Kilcik *et al.*, 2012; Feng *et al.*, 2015; Yan *et al.*, 2015), we fail to obtain the accurate pixel-by-pixel magnetic field features for each UD. Therefore, we used the mean magnetic flux of the periphery and the center of each umbra in our analysis. To improve the sensitivity of the mean flux density, the B_r maps were selected during the observed time interval of each data set and then averaged. Figure 6 shows two B_r maps that were from NOAA 11801 and 12158. The maps were extended to the same scale using a nearest-neighbor interpolation method and aligned to the corresponding corrected TiO image (*i.e.*, the image shown in Figure 3). In this figure, the periphery and center boundaries are superposed on the magnetic map with yellow and red curves, respectively. The mean flux densities of the periphery and the center according to the corresponding extended magnetic images are listed Table 5. Figure 7 show the relationships between magnetic flux density and CUD properties (diameter, intensity, lifetime, and

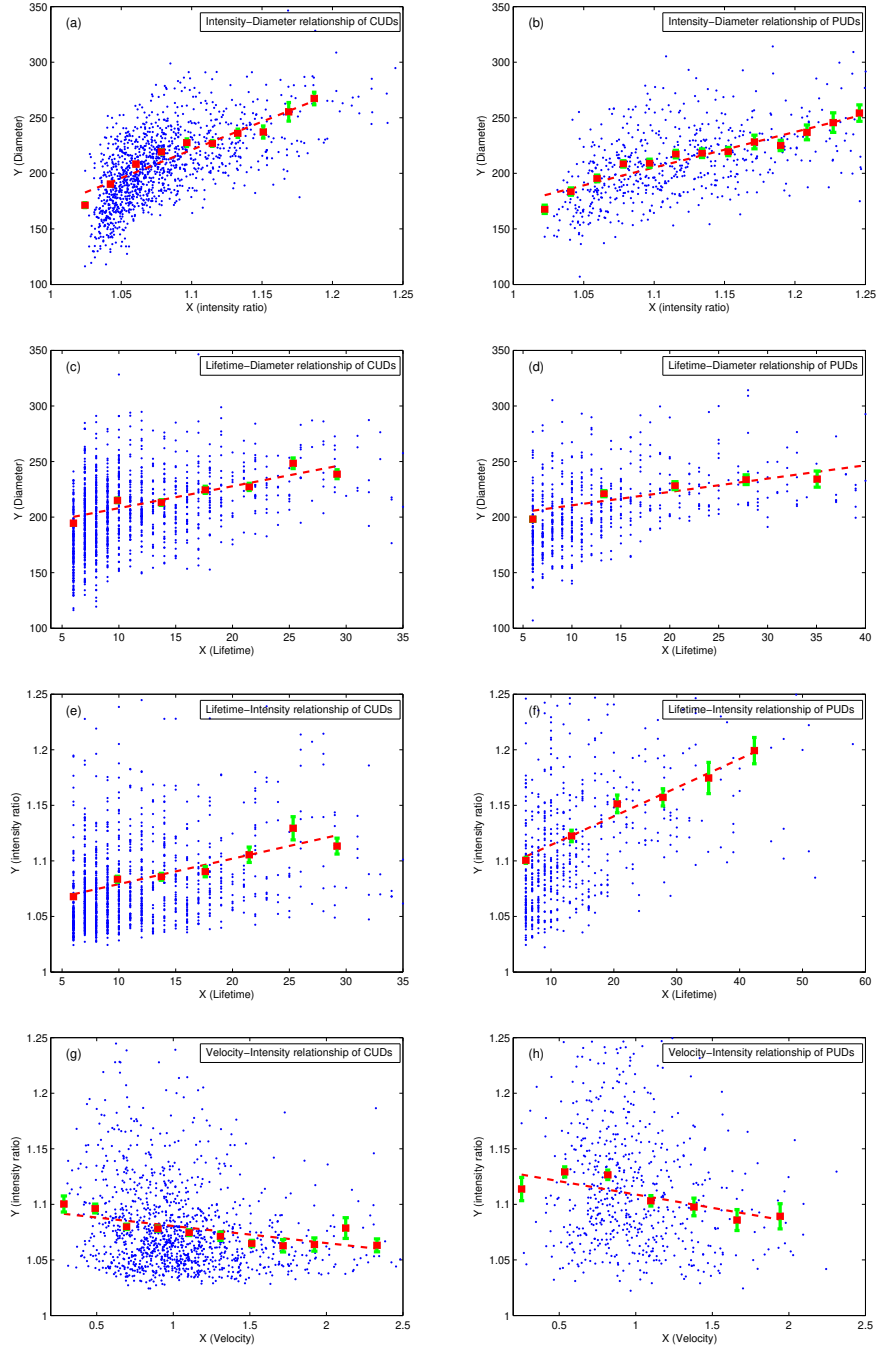


Figure 5. The scatter plots of all CUDs and all PUDs obtained for the four active regions. The left column illustrates the CUD relationships and the right column the PUD ones. (a–b) Corresponds to the intensity-diameter relationship, (c–d) to the lifetime-diameter, (e–f) to the lifetime-intensity, and (g–h) to the velocity-intensity one.

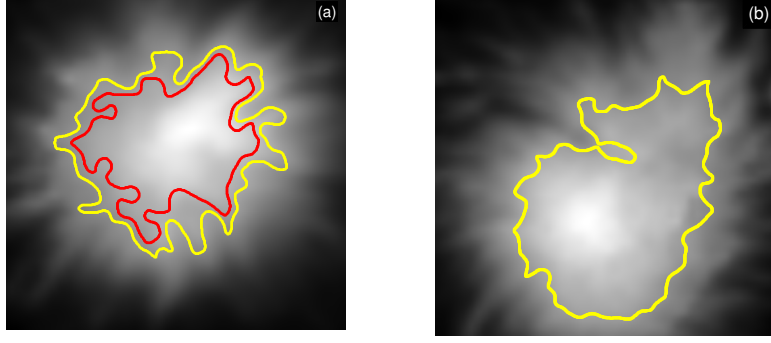


Figure 6. The radial component of the magnetic field B_r superposed on the umbra-penumbra and periphery-center boundaries with red and yellow curves: (a) B_r map of NOAA 11801 obtained with the SDO/HMI on 1 August 2013 at 03:48:00 UT. (b) B_r map of NOAA 12158 obtained on 13 September 2014 at 03:00:00 UT.

Table 5. The mean magnetic flux density of each umbra

CUDs						
AR NOAA	11598	11801	12158			12178
Spot			A	B	C	
Mean Flux Density	2334	2009	1566	2079	1741	2212
PUDs						
Mean Flux Density	1888	1582				1688

velocity). The green lines are the standard errors of each CUD data sets, and the red dash-lines are the fitted ones based on the six sunspots. Their correlation coefficients are -0.87, -0.91, -0.47, and 0.79. The PUD relationship is not shown because we only have three data sets. From the fitted lines in Figure 7 we can find that the diameters and the brightness of CUDs have a decreasing trend with increasing magnetic flux density (see Figures 7a and b), while the velocity increases with increasing flux density (see Figure 7d). However, the CUD lifetimes fail to exhibit an obvious trend with different magnetic flux densities (see Figure 7c). The results also imply that CUDs are larger and brighter and their motion slower in a reduced magnetic flux density; however, their lifetimes are unrelated to the flux density.

5. Conclusions

We selected high-resolution TiO image sequences of four ARs obtained under the best seeing conditions with the NVST to investigate UD properties and analyze the relationships between their different properties. The four ARs include six

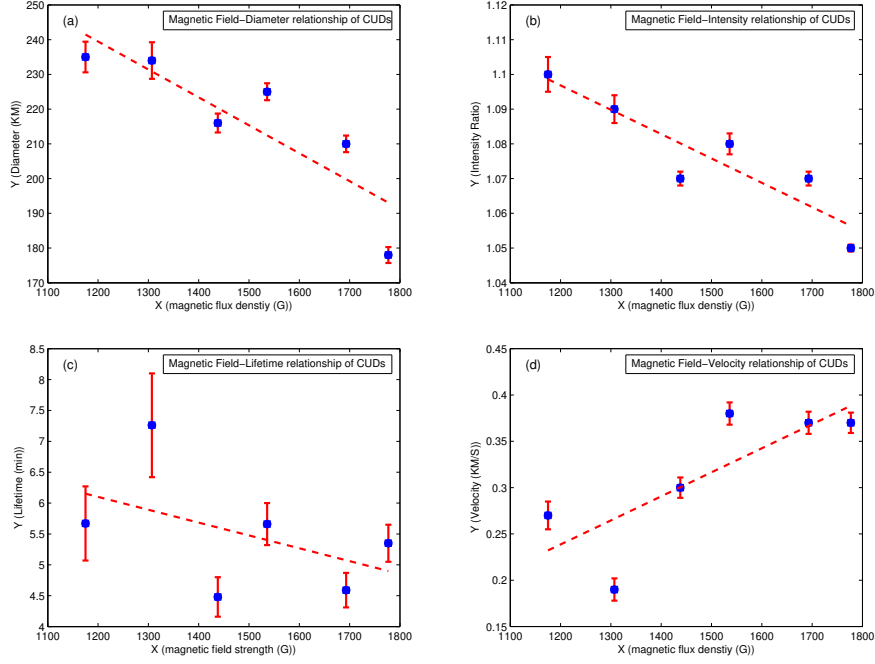


Figure 7. Relationships between magnetic flux density and CUD properties: (a) diameter–magnetic flux density plot, (b) intensity–magnetic flux density plot, (c) lifetime–magnetic flux density plot, and (d) velocity–magnetic flux density plot.

sunspots, and 1220 CUDs and 603 PUDs were identified from six and three sunspots, respectively. Subsequently, the magnetic field relation to UD properties was analyzed using the radial component of the magnetic field obtained from SDO/HMI images.

For an UD, regardless if it is a CUD or PUD, its diameter and lifetime holds an increasing trend with brightness, whereas its horizontal velocity exhibits an inverse trend. Its diameter becomes larger, and its brightness higher, and its velocity slower in a weak magnetic field than in a strong field. However, the lifetimes of UDs located in different sunspots are not obviously different, implying that the UD lifetime is unrelated to the magnetic flux density.

Note that PUD trends were obtained using the samples from three sunspots. Because CUDs and PUDs have different origins, formation height in the atmosphere, and dynamics, they represent different physical characteristics. The method, which divides UDs into CUDs and PUDs based on the umbral profile, could mix up both CUDs and PUDs and distort the statistical results.

Acknowledgements The authors are grateful to the referee for enlightening comments and suggestions that improved the quality of our work. This work is supported by the National Natural Science Foundation of China (Numbers: U1231205, U1531132, 11573012, 11463003, 11303011, 11263004, 11163004) and the Open Research Program of Key Laboratory of Solar Activity of the Chinese Academy of Sciences (Numbers: KLSA201414, KLSA201505). This

work is also supported by the Opening Project of the Key Laboratory of Astronomical Optics and Technology, Nanjing Institute of Astronomical Optics and Technology, Chinese Academy of Sciences (Number: CAS-KLAOT-KF201306). The authors thank the NVST team for their high-resolution observations.

References

- Berdugina, S.V., Solanki, S.K., Frutiger, C.: 2003, The molecular Zeeman effect and diagnostics of solar and stellar magnetic fields. II. Synthetic Stokes profiles in the Zeeman regime. *Astron. Astrophys.* **412**, 513–527. doi:10.1051/0004-6361:20031473.
- Bharti, L., Beeck, B., Schüssler, M.: 2010, Properties of simulated sunspot umbral dots. *Astron. Astrophys.* **510**, A12. doi:10.1051/0004-6361/200913328.
- Bharti, L., Joshi, C., Jaaffrey, S.N.A.: 2007, Observations of Dark Lanes in Umbral Fine Structure from the Hinode Solar Optical Telescope: Evidence for Magnetoconvection. *Astrophys. J. Lett.* **669**, L57–L60. doi:10.1086/523352.
- Feng, S., Deng, L., Shu, G., Wang, F., Deng, H., Ji, K.: 2012, A subpixel registration algorithm for low PSNR images. *2012 IEEE Fifth Int. Conf. on Advanced Computational Intelligence (ICACI)*, 626–630. IEEE.
- Feng, S., Xu, Z., Wang, F., Deng, H., Yang, Y., Ji, K.: 2014a, Automated Detection of Low-Contrast Solar Features Using the Phase-Congruency Algorithm. *Solar Phys.* **289**, 3985–3994. doi:10.1007/s11207-014-0538-2.
- Feng, S., Yu, L., Yang, Y.-F., Ji, K.-F.: 2014b, Identification of emission sources of umbral flashes using phase congruency. *Res. Astron. Astrophys.* **14**, 1001–1010. doi:10.1088/1674-4527/14/8/010.
- Feng, S., Zhao, Y., Yang, Y., Ji, K., Deng, H., Wang, F.: 2015, Identifying and Tracking of Peripheral and Central Umbral Dots. *Solar Phys.* **290**, 1119–1133. doi:10.1007/s11207-015-0670-7.
- Grossmann-Doerth, U., Schmidt, W., Schroeter, E.H.: 1986, Size and temperature of umbral dots. *Astron. Astrophys.* **156**, 347–353.
- Hamedivafa, H.: 2008, Application of an Improved Method of Image Segmentation and Some Considerations on Identification and Tracking of Umbral Dots. *Solar Phys.* **250**, 17–29. doi:10.1007/s11207-008-9201-0.
- Hamedivafa, H.: 2011, Kinematics of Umbral Dots: Their Typical Area, Brightness and Lifetime. *Solar Phys.* **270**, 75–88. doi:10.1007/s11207-011-9729-2.
- Kilcik, A., Yurchyshyn, V.B., Rempel, M., Abramenko, V., Kitai, R., Goode, P.R., Cao, W., Watanabe, H.: 2012, Properties of Umbral Dots as Measured from the New Solar Telescope Data and MHD Simulations. *Astrophys. J.* **745**, 163–176. doi:10.1088/0004-637X/745/2/163.
- Liu, Z., Xu, J., Gu, B.-Z., Wang, S., You, J.-Q., Shen, L.-X., Lu, R.-W., Jin, Z.-Y., Chen, L.-F., Lou, K., Li, Z., Liu, G.-Q., Xu, Z., Rao, C.-H., Hu, Q.-Q., Li, R.-F., Fu, H.-W., Wang, F., Bao, M.-X., Wu, M.-C., Zhang, B.-R.: 2014, New vacuum solar telescope and observations with high resolution. *Res. Astron. Astrophys.* **14**, 705–718. doi:10.1088/1674-4527/14/6/009.
- Lohmann, A.W., Weigelt, G., Wirtzner, B.: 1983, Speckle masking in astronomy - Triple correlation theory and applications. *Applied Optics* **22**, 4028–4037. doi:10.1364/AO.22.004028.
- Louis, R.E., Mathew, S.K., Bellot Rubio, L.R., Ichimoto, K., Ravindra, B., Raja Bayanna, A.: 2012, Properties of Umbral Dots from Stray Light Corrected Hinode Filtergrams. *Astrophys. J.* **752**, 109–118. doi:10.1088/0004-637X/752/2/109.
- Parker, E.N.: 1979, Sunspots and the physics of magnetic flux tubes. IX - Umbral dots and longitudinal overstability. *Astrophys. J.* **234**, 333–347. doi:10.1086/157501.
- Riethmüller, T.L., Solanki, S.K., Zakharov, V., Gandorfer, A.: 2008, Brightness, distribution, and evolution of sunspot umbral dots. *Astron. Astrophys.* **492**, 233–243. doi:10.1051/0004-6361:200810701.
- Schou, J., Scherrer, P.H., Bush, R.I., Wachter, R., Couvidat, S., Rabello-Soares, M.C., Bogart, R.S., Hoeksema, J.T., Liu, Y., Duvall, T.L., Akin, D.J., Allard, B.A., Miles, J.W., Rairden, R., Shine, R.A., Tarbell, T.D., Title, A.M., Wolfson, C.J., Elmore, D.F., Norton, A.A., Tomczyk, S.: 2012, Design and Ground Calibration of the Helioseismic and Magnetic Imager

- (HMI) Instrument on the Solar Dynamics Observatory (SDO). *Solar Phys.* **275**, 229–259. doi:10.1007/s11207-011-9842-2.
- Schüssler, M., Vögler, A.: 2006, Magnetoconvection in a Sunspot Umbra. *Astrophys. J. Lett.* **641**, L73–L76. doi:10.1086/503772.
- Sobotka, M., Bonet, J.A., Vazquez, M.: 1993, A High-Resolution Study of Inhomogeneities in Sunspot Umbrae. *Astrophys. J.* **415**, 832–846. doi:10.1086/173205.
- Sobotka, M., Brandt, P.N., Simon, G.W.: 1997a, Fine structure in sunspots. I. Sizes and lifetimes of umbral dots. *Astron. Astrophys.* **328**, 682–688.
- Sobotka, M., Brandt, P.N., Simon, G.W.: 1997b, Fine structure in sunspots. II. Intensity variations and proper motions of umbral dots. *Astron. Astrophys.* **328**, 689–694.
- Sobotka, M., Puschmann, K.G.: 2009, Morphology and evolution of umbral dots and their substructures. *Astron. Astrophys.* **504**, 575–581. doi:10.1051/0004-6361/200912365.
- Sobotka, M., Vázquez, M., Bonet, J.A., Hanslmeier, A., Hirzberger, J.: 1999, Temporal Evolution of Fine Structures in and around Solar Pores. *Astrophys. J.* **511**, 436–450. doi:10.1086/306671.
- Sun, X.: 2013, On the Coordinate System of Space-Weather HMI Active Region Patches (SHARPs): A Technical Note. *ArXiv: 1309.2392*.
- Tritschler, A., Schmidt, W.: 2002, Sunspot photometry with phase diversity. II. Fine-structure characteristics. *Astron. Astrophys.* **388**, 1048–1061. doi:10.1051/0004-6361:20020542.
- Tubbs, R.N.: 2004, Lucky exposures: diffraction-limited astronomical imaging through the atmosphere. *The Observatory* **124**, 159–160.
- Watanabe, H., Kitai, R., Ichimoto, K.: 2009, Characteristic Dependence of Umbral Dots on Their Magnetic Structure. *Astrophys. J.* **702**, 1048–1057. doi:10.1088/0004-637X/702/2/1048.
- Watanabe, H., Bellot Rubio, L.R., de la Cruz Rodríguez, J., Rouppe van der Voort, L.: 2012, Temporal Evolution of Velocity and Magnetic Field in and around Umbral Dots. *Astrophys. J.* **757**, 49–74. doi:10.1088/0004-637X/757/1/49.
- Xu, Z., Jin, Z.Y., Xu, F.Y., Liu, Z.: 2014, Primary observations of solar filaments using the multi-channel imaging system of the New Vacuum Solar Telescope. In: Schmieder, B., Malherbe, J.-M., Wu, S.T. (eds.), *IAU Symposium*, **300**, 117–120. doi:10.1017/S1743921313010831.
- Yan, X.L., Xue, Z.K., Pan, G.M., Wang, J.C., Xiang, Y.Y., Kong, D.F., Yang, L.H.: 2015, The Formation and Magnetic Structures of Active-region Filaments Observed by NVST, SDO, and Hinode. *Astrophys. J. Suppl. Ser.* **219**, 17–35. doi:10.1088/0067-0049/219/2/17.
- Yang, Y.-F., Qu, H.-X., Ji, K.-F., Feng, S., Deng, H., Lin, J.-B., Wang, F.: 2015, Characterizing motion types of G-band bright points in the quiet Sun. *Res. Astron. Astrophys.* **15**, 569–582. doi:10.1088/1674-4527/15/4/009.
- Zhou, L., Li, C.-S.: 1998, *Electronic Imaging and Multimedia Systems II, Proc. SPIE* **3561**.